

Assessment of Laser-Induced Damage in Laser-Micromachined Rare-Earth Permanent Magnets

Brock A. Peterson¹, Florian Herrault¹, Ololade D. Oniku², Zachary A. Kaufman², David P. Arnold², and Mark G. Allen¹, *Fellow, IEEE*

¹MicroSensors and MicroActuators Group and the School of Electrical and Computer Engineering, Georgia Institute of Technology, Atlanta, GA 30332 USA

²Interdisciplinary Microsystems Group and Dept. of Electrical and Computer Engineering, University of Florida, Gainesville, FL 32611 USA

The effects of micromachining bulk rare-earth magnets are investigated by measurements of the moment of sub-millimeter scale micromachined structures. A model representing these effects is also presented to provide a basis for interpreting the results. Laser-induced damage to the magnetic material, manifesting as a loss of magnetic properties, is estimated to reach 10–20 μm from the magnet edge in the lateral dimension. The results indicate the affected volume due to laser micromachining bulk rare-earth magnets is limited to less than 25 μm , laterally through the material, for the rare-earth magnetic materials tested.

Index Terms—Laser micromachining, micromagnets, NdFeB, remanence, SmCo.

I. INTRODUCTION

HIGH-ENERGY-PRODUCT rare-earth magnetic materials such as SmCo and NdFeB alloys have enabled or enhanced many application areas. In recent years, smaller application areas such as microelectromechanical systems (MEMS) and biomedical devices have fueled interest in sub-millimeter microstructured magnets, where the overall magnet size or features on the magnet may range from micrometers to hundreds of micrometers. In addition, some applications of MEMS devices require a high spatial frequency magnetic field. An example of such a structure is shown in Fig. 1. Fig. 1 shows one assembled SmCo laser micromachined comb array exhibiting an alternating magnetic field. Applications include permanent magnet microgenerators, actuators, microundulators, etc. However, there is a lack of manufacturing methods for realizing high-performance magnets with these dimensions [1].

Traditional manufacturing of the best performing rare-earth magnets involves the bonding and/or sintering of fine powders in cavities or molds that define the magnet size and shape. These powder metallurgy approaches are generally limited to dimensional features with size scales down to about 1 mm. A review of permanent magnet processing and materials in MEMS, performed by Arnold *et al.*, shows some of the highlights of permanent magnets at dimensions below 1 mm and some of the challenges to their fabrication. To realize these fine microstructured magnets, there are generally two alternatives to bulk manufacturing: develop alternative ways to synthesize magnetic materials, or determine how to selectively subtract material from bulk magnets to create the desired scale forms. Example “bottom-up” approaches include evaporation, sputtering, electrodeposition, pulsed-laser deposition,

Manuscript received March 02, 2012; accepted April 10, 2012. Date of current version October 19, 2012. Corresponding author: B. A. Peterson (e-mail: brock.peterson@gatech.edu).

Color versions of one or more of the figures in this paper are available online at <http://ieeexplore.ieee.org>.

Digital Object Identifier 10.1109/TMAG.2012.2196423

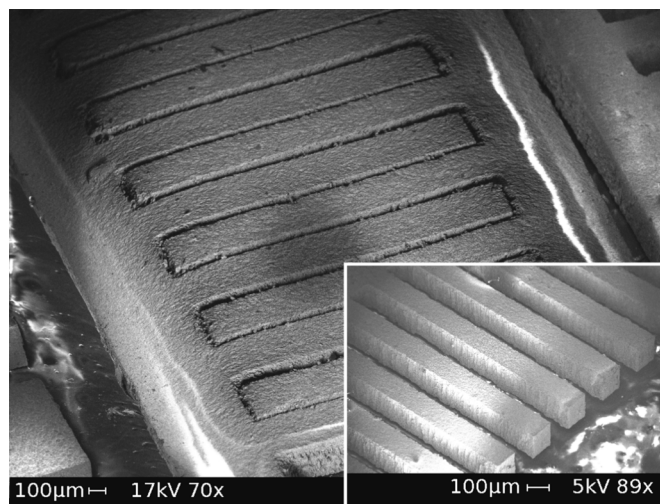


Fig. 1. Scanning electron microscopy (SEM) image of a highly spatially varying, alternate pole magnetic field assembly, the period of which is 500 μm . Inset image is an SEM of one side of the array.

screen-printing of powders, and others. However, most of these methods result in materials with limited energy-product, as compared to bulk magnets. The alternative “top-down” approaches include methods such as grinding, chemical etching, laser-micromachining, and electric discharge machining [1], [2].

Laser-micromachining is an effective and reasonably high-speed manufacturing method for achieving fine-scale mechanical structures. Laser machining relies on ablation of material using high-energy laser pulses. One drawback is that the laser ablation process typically generates a large amount of heat and may leave a magnetically “damaged zone” along the laser cutting path. For magnetic materials, this damaged zone likely no longer possesses strong magnetic properties, if any. Hence, assessment of this damaged zone is critical for understanding the applicability of laser-micromachining, especially for small-scale structures, where the physical size of

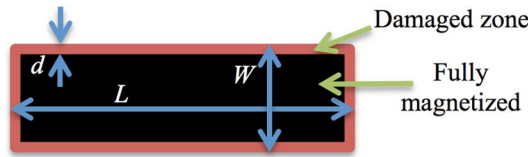


Fig. 2. Schematic of a laser micromachined magnet sample. Typical sizes are $L = 2$ mm, $W = 500 \mu\text{m} - 50 \mu\text{m}$, and thickness (extruded image) = 300 or 500 μm . Samples are magnetized through the thickness.

the structures may approach the physical size of the damaged zone.

In this paper, general degradation effects (due to oxidation, extreme heat, or other effects) caused by laser micromachining bulk samarium-2-cobalt-17 (SmCo) and neodymium-iron-boron (NdFeB) are investigated by use of a phenomenological model applied to test structures of appropriate scale.

II. MODEL

A. Model Description

In order to better understand the limits of laser machining, a simple model was constructed. Consider the laser micromachining of a single rectangular piece of magnetic material from a much larger sheet as shown schematically in Fig. 2. The nominal volume of this piece is

$$V_0 = LWT \quad (1)$$

where L is the length, W is the width, and T is the thickness. If we assume a damage zone d extends into the piece at all points immediately adjacent to the beam, the width and length are slightly reduced but the thickness is not. The effective volume of the magnet is V' , which is defined as

$$\begin{aligned} V' &= (L - 2d)(W - 2d)T \\ &= WLT - 2dLT - 2dWT + 4d^2T. \end{aligned} \quad (2)$$

Neglecting terms in d^2 , assuming d is small, we obtain

$$V' = V_0 - 2dLT - 2dWT. \quad (4)$$

The percent useful volume can then be defined as V'/V_0 .

Assumptions included in this model consist of a completely demagnetized (100% damaged) region adjacent to the laser cut that cannot be remagnetized. The magnetic pieces are assumed to be in the shape of a rectangular prism as shown in Fig. 2. Taking V' and V_0 , (4) and (1), as a ratio, yields

$$V'/V_0 = -2d \cdot (1/W) + (1 - 2d/L). \quad (5)$$

Equation (5) suggests that for a sequence of rectangular prisms of differing width, but the same length and thickness, a plot of the percentage volume of the magnet that can still be magnetized as a function of the reciprocal of the width ($1/W$) should

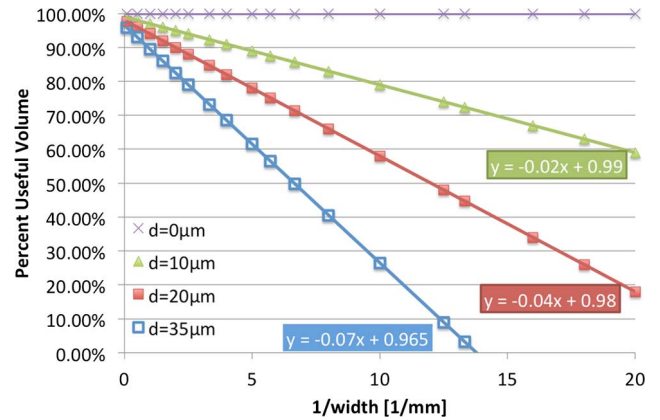


Fig. 3. Phenomenological model of multiple damage zones with varying magnet widths.

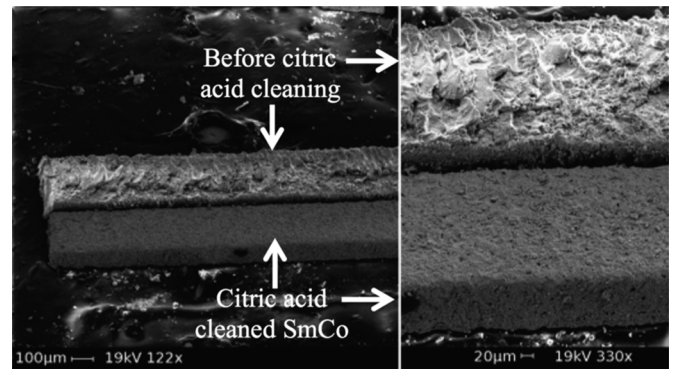


Fig. 4. SEM of two laser-machined SmCo pieces for VSM before (top) and after (bottom) cleaning. The right image is a close-up view. Piece dimensions: 100 $\mu\text{m} \times 300 \mu\text{m} \times 2$ mm.

be linear, with slope related to twice the size of the damaged zone. Equation (5) is illustrated graphically in Fig. 3, for a hypothetical experiment of microfabricated pieces ranging from $W = 2$ mm to $W = 35 \mu\text{m}$ as parameterized by damaged zone extent d .

As seen in Fig. 3, if the extent of the damaged zone as a result of laser micromachining is zero (the ideal case), measurement of the magnetization ($\mu_0 M_r$) as a function of inverse width would result in a line of zero slope stretching from $1/W = 0$ to $1/W = \infty$. All points along that line would have a magnetization equal to the magnetization of the bulk magnetic material. However, should the extent of the damaged zone be nonzero, a reduction in magnetization is observed as the width of the magnet decreases, since the magnet is composed of higher percentages of damaged material as the width decreases.

B. Simulation Results

Plotting equation (5) versus $1/W$ with a fixed damage zone and length expectedly gives a straight line with a negative slope ($m = -2d$, shown in Fig. 3). From the slope we extract the damage zone, d . It should be noted that the x-intercept of this line is the point at which no remanent magnetization is left in the magnetic material.

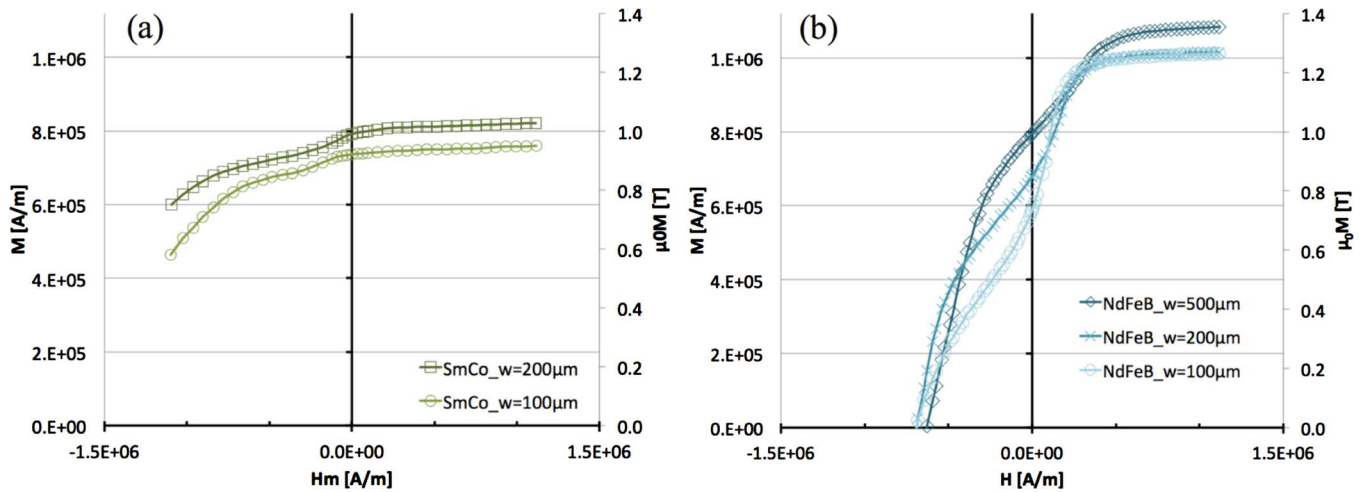


Fig. 5. VSM demagnetization curves for (a) 300 μm thick SmCo and (b) 500 μm thick NdFeB laser-micromachined magnets with varying widths.

III. EXPERIMENTAL

A. Methods and Assumptions

Each of the magnetic samples was laser micromachined (Laser 1: Nd:YLF IR laser, pulse width = 100 μs , pulse period = 1 ms, cut speed = 30–40 $\mu\text{m/s}$, with air assist above and vacuum underneath; Laser 2: Coherent Talisker picosecond laser, 355 nm wavelength, pulse frequency = 200 kHz and pulse width = 10–15 ps, cut speed = 100 mm/s) from bulk pieces of either NdFeB or SmCo of thickness 500 or 300 μm . Samples were cut to lengths of $L = 2$ mm, with nominal widths ranging from $W = 1$ mm to $W = 50$ μm . Generally, two or more pieces of each width were cut. The samples were cleaned, either with a soft paper, citric acid, or 400-grit sandpaper, before accurately measuring the dimensions and weighing. Each piece was then measured on a microscope with encoders and weighed on a microgram scale. The magnetic pieces were then attached to a small glass slide cover under a microscope. This was done to align the out-of-plane magnetization. The adhesive used is a low temperature thermoplastic material (Crystalbond 555 or 505) for protection and to prevent movement/vibration. The assembled slide pieces were then attached to a vibrating sample magnetometer (VSM) insert, magnetized in a pulse magnetizer at a field strength nominally sufficient to fully magnetize the pieces (Oersted Technologies, Magnetizer 340B, $B > 3.5$ T) or a high field strength superconducting magnet (Bruker DSX 300, $B_0 = 7$ T), and measured in a VSM (Lake Shore Cryotronics, 7304 Series VSM System, $H_{\text{applied,max}} = 1120$ kA/m = 14 kOe; ADE EV9 VSM, $H_{\text{applied,max}} = 2000$ kA/m = 25 kOe). This provided at least three data points for each size of sample.

B. Sample Variation

As mentioned in the previous section, the samples were cleaned prior to measuring and assembly. This was to aid in measurement of physical dimensions and to obtain an accurate mass without contaminating materials adhering to the surface of the magnets. The NdFeB and the SmCo were initially rubbed clean on a cloth to remove loose debris. This left a substantial amount of firmly attached, redeposited material on the surface

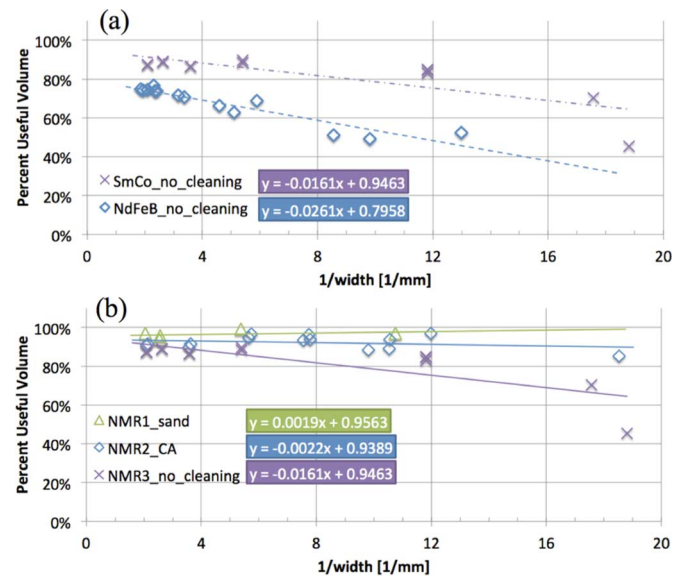


Fig. 6. (a) Plot of percent useful magnetic volume as a function of width for NdFeB and SmCo with fit lines and line equations. The damaged depth into the material is extracted as half the slope of each line ($d_{\text{SmCo}} \sim 8$ μm , $d_{\text{NdFeB}} \sim 13$ μm). (b) Similar plot of percent useful magnetic volume comparing the use of cleaning agents to no cleaning at all for similar SmCo pieces. CA indicates that the set was cleaned with citric acid, sand indicates that the set was sanded with 400 grit sandpaper, and no_cleaning indicates that the set was only lightly brushed to remove loose particles.

of the samples, which introduced some error in physical dimension and mass measurements due to variations between magnet samples. To address this, the SmCo samples were cleaned in a 15% citric acid solution at 80 $^{\circ}\text{C}$ or gently rubbed on 400-grit sandpaper. Fig. 4 shows differences between laser-machined pieces soon after machining as well as after cleaning with citric acid.

IV. RESULTS AND DISCUSSION

Fig. 5 shows the demagnetization curves of the magnetic pieces of SmCo [see Fig. 5(a)], and NdFeB [see Fig. 5(b)]. The ratio of the magnetization at zero applied field to the nominal magnetization of the bulk material is taken as a surrogate

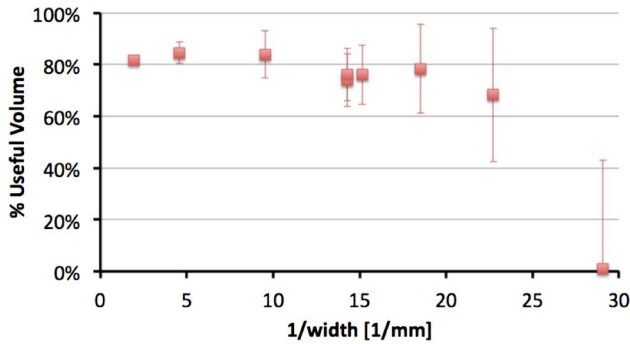


Fig. 7. Plot similar to Fig. 6 of SmCo without any cleaning with the addition of very small ($W \sim 40 \mu\text{m}$) pieces. To the far right ($1/W = 29$) is a sample with some soft ferromagnetic properties.

TABLE I
BULK PROPERTIES OF MAGNETIC MATERIALS USED

Property	NdFeB N48	SmCo 30/25
Remanent Magnetization, $\mu_0 M_r$	1.38 T	1.07-1.12 T
Coercivity, H_c	$\geq 867 \text{ kA/m}$, $\geq 10.90 \text{ kOe}$	$\geq 704 \text{ kA/m}$, $\geq 8.8 \text{ kOe}$
Intrinsic Coercivity, H_{ci}	$\geq 955 \text{ kA/m}$, $\geq 12.0 \text{ kOe}$	$\geq 2000 \text{ kA/m}$, $\geq 25.0 \text{ kOe}$
Energy-Product, $(BH)_{max}$	370-390 kJ/m^3 46-49 MGOe	225-250 kJ/m^3 28-31 MGOe

for the ratio of effective volume to total volume of (5), or the percentage of useful volume of magnetic material in the laser micromachined pieces. These ratios are not corrected for geometric demagnetization factors as [3] suggests for similar rectangular prisms, due to the complexity of using an unknown damaged volume of material in the calculation. The kinks in the demagnetization curves were observed with cleaved virgin magnetic material as well as micromachined pieces of all sizes and are therefore not attributed to processing.

Fig. 6 shows the percentage of useful volume plotted as a function of inverse width according to the phenomenological model of (5). As seen, a downward slope is observed in the regime of the larger reciprocal widths, which is where the effect of the damage zone is likely to be most pronounced. The data show that both NdFeB and SmCo respond favorably to laser micromachining when sample widths are greater than three times the damage zone ($W \geq 3d$). The data suggest that both NdFeB and SmCo have damage zones of approximately $10\text{--}20 \mu\text{m}$. The laser-damaged volume appears to be greater in the NdFeB material than in the SmCo, shown in Fig. 6(a). A y-intercept offset also appears in Fig. 6(a) that is not well understood, but could be due to heat affecting the bulk of the material in the NdFeB. The change in slope between NdFeB and SmCo is likely due to the large difference in Curie temperature ($310 \text{ }^\circ\text{C}$ and $825 \text{ }^\circ\text{C}$, respectively) and reversible temperature coefficient of re-

manence ($-0.1\%/^\circ\text{C}$ and $-0.03\%/^\circ\text{C}$, respectively) as well as possibly being affected by the thermal conductivity (penetration efficiency into the material) and specific heat of the materials [1], [4].

In Fig. 6(b), the plot compares the use of citric acid cleaning to sanding the material edges to no cleaning agents used for SmCo pieces. It is interesting to note that the slopes vary substantially between those pieces cleaned and not cleaned. It is possible that the laser is inducing multiple types of damage during the micromachining process: 1) mechanical and 2) magnetic damage. If this is the case, it can be reasoned that the uncleaned piece sets exhibit both the mechanical and magnetic damage. Whereas, the citric acid cleaned pieces appear to exhibit less damage, likely magnetic damage as the mechanical debris (oxidation and redeposition) is removed with citric acid. The lightly sanded pieces appear to exhibit no damage or loss in magnetization down to small widths [a slightly positive slope on the $1/W$ graph in Fig. 6(b)], likely due to the removal of the mechanical debris and part or all of the thin damaged zone. It should be noted that mechanical sanding, no matter how light, is a destructive and laborious method of cleaning, and is not feasible for use in batch processing and other MEMS fabrication methods. However, sandblasting could be a suitable alternative with a similar result. Fig. 7 further shows that very small widths, difficult to produce and measure without breaking, can show a remanent magnetization of zero while maintaining some of the material magnetic properties, such as slightly higher permeability and saturation.

V. CONCLUSION

Laser micromachining proves to be a promising magnet microfabrication method to achieve high energy-product magnetic structures on the sub-millimeter scale. Laser micromachined dimensions can reach below $100 \mu\text{m}$ allowing for future integration in MEMS, especially for multi-pole magnetic structures that require a highly spatially varying magnetic field.

ACKNOWLEDGMENT

This work was supported in part by the U.S. Department of Defense, DARPA AXiS Program under Grant N66001-11-1-4198. The authors would like to thank Mr. R. Shafer for assistance with laser machining.

REFERENCES

- [1] D. P. Arnold and N. Wang, "Permanent magnets for MEMS," *J. Microelectromech. Syst.*, vol. 18, no. 6, pp. 1255–1266, July 2009.
- [2] F. Herrault, C. H. Ji, and M. G. Allen, "Ultraminaturized, high-speed, permanent-magnet generators for milliwatt-level power generation," *J. Microelectromech. Syst.*, vol. 17, no. 6, pp. 1376–1387, 2008.
- [3] A. Aharoni, "Demagnetizing factors for rectangular ferromagnetic prisms," *J. Appl. Phys.*, vol. 83, no. 6, pp. 3432–3434, Mar. 1998.
- [4] Arnold Magnetic Technologies Corporation, Rochester, NY, "Product Specifications," 2012. [Online]. Available: <http://www.arnoldmagnetics.com>